Chapter 4
A Comparison of the Model Parameter Estimations from Self-Potential Anomalies by Levenberg-Marquardt (LM), Differential Evolution (DE) and Particle Swarm Optimization (PSO) Algorithms: An Example from Tamış-Çanakkale, Turkey

Petek Sindirgi and Şenol Özyalin

Abstract In geophysics, it is particularly important to choose an adequate optimization algorithm for parameter estimation. In this study, the success of Levenberg-Marquardt (LM), Differential Evolution (DE) and Particle Swarm Optimization (PSO) inversion algorithms has been tested by applying to the synthetic and field self-potential (SP) anomalies. Even though it is not preferred to compare derivative-based algorithms with metaheuristics, thanks to a LM-based limitation procedure first proposed in this study, a comparison could be realized. First, a synthetic SP data have been inverted by LM, DE and PSO algorithms. Then, SP field data set collected from Tamış-Çanakkale, Turkey was evaluated by the same algorithms. The estimated model parameters by these algorithms were compared with each other. We also inverted vertical electrical sounding (VES) data set collected from the same region, and an earth model was constructed by using both SP and VES methods. The results from each geophysical method point out the same location for a fault. Based on these studies, it can be concluded that DE, PSO, and LM algorithms may be confidently used in SP modelling studies.

Keywords Differential evolution · Levenberg-Marquardt · Particle swarm optimization · Self-potential · Vertical electrical sounding

P. Sindirgi (✉) · Ş. Özyalin
Faculty of Engineering, Department of Geophysical Engineering, Dokuz Eylül University, İzmir, Turkey
e-mail: petek.sindirgi@deu.edu.tr

Ş. Özyalin
e-mail: senol.ozyalin@deu.edu.tr

A. Biswas (ed.), *Self-Potential Method: Theoretical Modeling and Applications in Geosciences*, Springer Geophysics, https://doi.org/10.1007/978-3-030-79333-3_4

4.1 Introduction

Electrical methods are frequently used to detect the location of systems including the groundwater. Self-potential (SP) and vertical electrical sounding (VES) are proven methods to be successful in groundwater explorations such as groundwater pollution studies, fresh, saltwater interference problems, and geothermal exploration (Ogilvy et al. 1969; Corwin and Hoover 1979; Schiavone and Quarto 1984; Hamzah et al. 2007; Karlık and Kaya 2001).

The VES technique is used to determine the resistivity changes from the surface to the depth. It is mainly based on the principle of measuring the response of the earth to an electric current applied to the ground. The VES method is useful in determining the depth, geometry and resistivity of the layers (Hamzah et al. 2007; Kaya et al. 2015).

Self-potential is an electrical phenomenon that is so easy to measure but it is also so hard to determine the source mechanism. These mechanisms can be specified as electro-kinetic (streaming), thermo-electric, diffusion, and electro-chemical potential. Self-potential method can be applied for determining the possible faults containing fluid in the study area (Yüngül 1950; Fitterman and Corwin 1982; Corwin 1990; Monteiro Santos et al. 2002; Revil et al. 2003). Potential anomalies created by fluid-containing faults are generally generated by electro-chemical sources.

SP anomalies can be analysed by different approaches. Since the use of the graphic-based evaluation methods (Yüngül 1950; Paul 1965; Rao et al. 1970), a new generation numerical methods have been developed for the evaluation of SP data in parallel with developing computer technology: The Fourier, Hartley, Hilbert Transforms and Wavelet analysis (Sundararajan et al. 1990; Asfahani et al. 2001; Gilbert and Pessel 2001; Al-Garni and Sundararajan 2011; Di Maio et al. 2016), Euler Deconvolution (Agarwal and Srivastava 2009; Sındırgı and Özyalın 2019), Gradient and Derivative Analysis (Abdelrahman et al. 1997, 1998, 2006; El-Araby 2004; Essa et al. 2008; Sındırgı et al. 2008; Abedi et al. 2012; Mehanee 2015), tomographic approach (Di Maio and Patella 1994; Patella 1997; Revil et al. 2001; Juliano et al.,2002), Artificial Neural Network algorithms (El-Kaliouby and Al-Garni 2009; Kaftan et al. 2014), and metaheuristic algorithms including Particle Swarm Optimization (PSO) (Juan et al. 2010, Monteiro Santos 2010; Göktürkler et al. 2016; Ekinci et al. 2019; Pekşen et al. 2011), Simulated annealing (SA) (Sharma 2012; Biswas and Sharma 2014, 2015), Genetic Algorithm (GA) and Differential Evaluation (DE) (Abdelazeem and Gobashy 2006; Fernández-Martínez et al. 2010; Göktürkler and Balkaya 2012; Di Maio et al. 2017; Ekinci et al. 2019).

In this study, a synthetic (noise-free and noisy) and a field SP data set (collected from Tamış-Çanakkale, Turkey) have been evaluated by three algorithms including the Levenberg-Marquardt (LM), PSO and DE. Also, to be able to compare LM to the metaheuristics, a new initial model selection process for LM was developed. Then, the estimated parameters have been compared with each other. The VES data set, collected from the same location, is also inverted, and the subsurface model for Tamış-Çanakkale anomaly has been constructed by combining the results from both VES and SP data.

4.2 Materials and Methods

4.2.1 Formulation of the SP Anomaly

Let $V(x, x_0, z_0, K, \theta, q)$ be the SP anomaly produced by a simple polarized causative body observed at any point on the earth's surface (Fig. 4.1). Formulation of the SP anomaly (Yüngül 1950; Murty and Haricharan 1985) can be written as;

$$V(x, x_0, z_0, K, \theta, q) = K \frac{(x - x_0)cos\theta + z_0 sin\theta}{\left[(x - x_0)^2 + z_0^2\right]^q} \tag{4.1}$$

where K is the electric dipole moment, x is the horizontal distance, x_0 is the distance from the origin, z_0 is the depth of the centre of the body, θ is the polarization angle, and q is the shape factor. The shape factor is dimensionless and its value for a sphere, horizontal cylinder, and semi-infinite vertical cylinder are 1.5, 1.0, and 0.5, respectively. The shape factor becomes near to zero as the structure approaches a horizontal sheet.

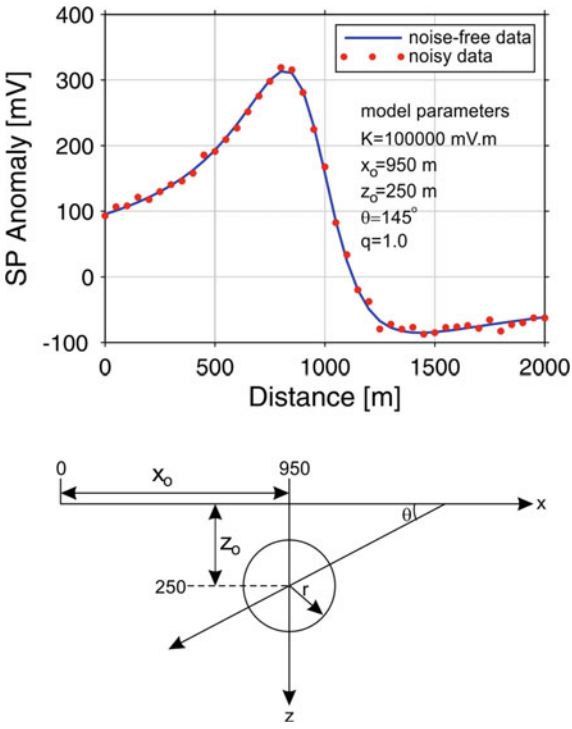

Fig. 4.1 An infinitely long horizontal cylinder model and its noise-free and noisy anomalies (The model parameters and their corresponding values are listed on the figure)

4.2.2 Algorithms

4.2.2.1 Levenberg-Marquardt (LM) Inversion Algorithm

Nonlinear least squares problems can be solved using the LM algorithm. The solution from the LM algorithm is not necessarily to be a global minimum. Generally, the LM algorithm is often preferred to Gauss-Newton and Steepest-Descent methods because it guarantees good convergence and non-singularity of the solution. Kenneth Levenberg introduced this algorithm in (1944), and Donald Marquardt (1963) improved it subsequently.

Generalized formulation of forward modelling problems can be written as,

$$\boldsymbol{d} = \mathrm{G}(\boldsymbol{m}) \tag{4.2}$$

where $\boldsymbol{d}$ is the M-dimensional vector of observations and, $\boldsymbol{m}$ is a vector of model parameters (in previous study model parameters are x_0, z_0, K, θ, q) with the size of N×1. G($\boldsymbol{m}$) is a nonlinear function predicted by the model. Model parameter $\boldsymbol{m}$ can be written by

$$\boldsymbol{m} = \boldsymbol{m}_0 + \Delta\boldsymbol{m} \tag{4.3}$$

where $\boldsymbol{m}_0$ is the initial model and $\Delta\boldsymbol{m}$ is the model parameters update.

Minimizing the model perturbation to the Gauss-Newton solution can be fulfil via minimizing the objective F,

$$\mathrm{F} = (\boldsymbol{d} - \mathrm{G}(\boldsymbol{m}_0 + \Delta\boldsymbol{m})) + \lambda\Delta m^2 \tag{4.4}$$

The sensitivity (Jacobian) matrix *J(M×N)* can be written as,

$$J = \begin{bmatrix} \frac{\partial G_i(m)}{\partial m_1} & \cdots & \frac{\partial G_i(m)}{\partial m_N} \\ \vdots & \ddots & \vdots \\ \frac{\partial G_M(m)}{\partial m_1} & \cdots & \frac{\partial G_M(m)}{\partial m_N} \end{bmatrix}$$

and using sensitivity matrix, $\Delta\boldsymbol{m}$ can be defined as

$$\Delta\boldsymbol{m} = \left[\boldsymbol{J}^T\boldsymbol{W}\boldsymbol{J} + \boldsymbol{I}\right]^{-1}\boldsymbol{J}^T\boldsymbol{W}(\boldsymbol{d} - \mathrm{G}(\boldsymbol{m}_0)) \tag{4.5}$$

where $\boldsymbol{I}$ is the identity matrix and λ is a damping factor shows the effect of model perturbation. If λ is small, Eq. (4.4) will become equal to Gauss-Newton solution equation. Generally, the initial value of λ is chosen large. If misfit is smaller than previous iteration λ is reduced, if not it is increased.$\boldsymbol{W}$ is a positive definite matrix and defined as (Jupp and Vozoff 1975)

$$\boldsymbol{W} = \frac{1}{\mathrm{M}}\boldsymbol{d}_i^2, \quad i = 1, 2, \ldots, \mathrm{M} \tag{4.6}$$

RMSE, which means the standard deviation of the residuals, is calculated as follows (Barnston 1992):

$$\mathrm{RMSE} = \sqrt{\frac{1}{\mathrm{M}}\sum_{i=1}^{\mathrm{M}}(\boldsymbol{d}_i - \mathrm{G}(\boldsymbol{m})_i)^2} \tag{4.7}$$

4.2.2.2 Particle Swarm Optimization (PSO) Algorithm

The PSO was proposed in 1995 by the authors Kennedy and Eberhart. It is a population-based metaheuristic technique and is based on the social behaviour of animals (birds, fishes). While each individual searching for the solution in PSO is called a *particle*, the population of the particles is called a *swarm*. Particles move according to two important parameters in the search space. *Pbest* is the particle's best position found so far and *Gbest* is global best position found thus far in the entire swarm. According to these definitions, basic steps of the PSO algorithm can be listed as follows: (1) The algorithm is initialized by placing the particles with random velocities (v) and positions (x) in the search space. (2) *The fitness value* is used to understand how close a particle is to the solution. It is calculated for each particle. (3) Individual and global bests are updated by comparing them with the previous ones ($\mathrm{pbest_i}$) and equalized to the current value of the fitness. Then the particle's prior best position (p_i) is assumed to be as the current position (x_i). The determined position of the particle with the best fitness value so far is assigned as the global best (g_i). (4.4) New velocity and position values are updated for each particle. (4.5) Stopping criterion is checked, if could not reach the threshold values, it is continued with step (4.2) (Fig. 4.2).

The position and velocity of a particle i can be updated as follows (i = 1, 2, 3, …, N);

$$v_i = \omega v_i + c_1 rand()(p_i - x_i) + c_2 rand()(g_i - x_i) \tag{4.8}$$

$$x_i = x_i + v_i \tag{4.9}$$

where w is a weighting factor ($0 < \omega < 1$) known as inertia weight; c_1 and c_2 are individual and social behaviour coefficients, respectively. *rand*() is a function to generate pseudo-random numbers within [0, 1]. The updates of position and velocity of each particle end after reaching the stopping criterion (Kennedy and Eberhart 1995; Shi and Eberhart 1998; Poli et al. 2007; Luke 2009; Salmon 2011). In the light

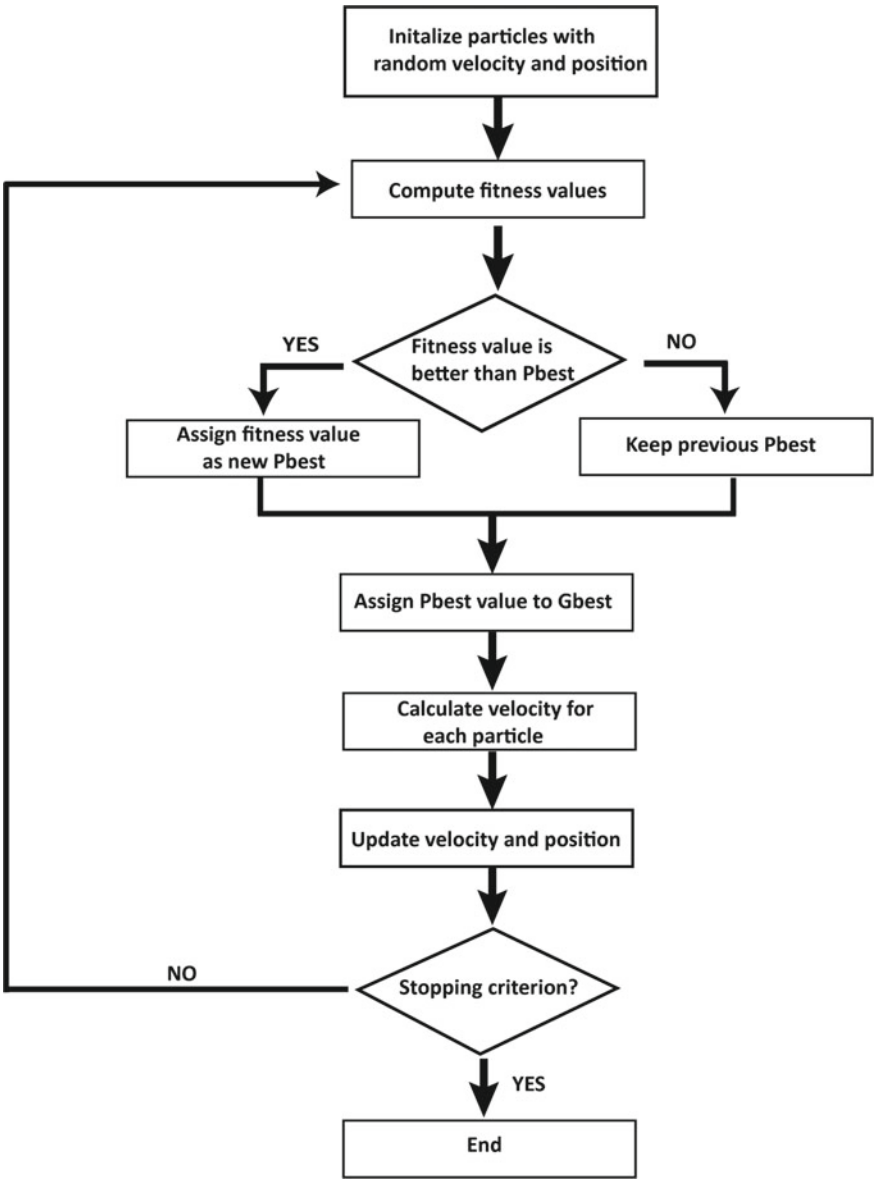

Fig. 4.2 The flow chart of the particle swarm optimization (Adopted from http://mnemstudio.org/particle-swarm-introduction.htm)

Table 4.1 The values of the parameters used in PSO and DE algorithms

DE parameters	Values	PSO parameters	Values
Number of parameter (D)	5	Number of parameter (D)	5
Population size and Weighting factor (F)	100 0.7	Particle number Inertia weight (ω)	100 1
Max. generation number (G)	100	Max. generation number (G)	100
Max. number of run	10	Max. number of run	10
Value to reach (VTR) (mV)	1e-11	Value to reach (VTR) (mV)	1e-11
Crossover probability (Cr)	0.9	Cognitive and social scaling factors (c1 and c2)	$c1 = 2$ $c2 = 2$

of this information, the values of the parameters used in PSO algorithm in this study are listed in Table 4.1.

4.2.3 Differential Evolution (DE) Algorithm

DE algorithm (Storn and Price 1995, 1997) is a population-based optimization algorithm and its applications in geophysics have increased in recent years. Different from the conventional gradient-based inversion methods, a good starting model is not a requirement for the DE algorithm to reach the global minimum. Three control parameters are the only requirements: number of population (Np), weighting factor (mutation constant, F) and crossover probability (Cr). The initial population is generated randomly in the initialization stage of the algorithm, then in the evolution stage population evolves from one generation to the next through mutation, crossover and selection operations until the termination criterion is satisfied (Fig. 4.3) (Li and Yin 2012; Ekinci et al. 2016).

The target vectors can be defined as $x_{i,G} = \left(x_{i,G}^1, x_{i,G}^2, \ldots, x_{i,G}^D\right), i = 1, 2, \ldots, Np$, where G is the current generation, and D is the number of parameters ($j = 1, 2, \ldots, D$). The jth component of the ith vector can be generated as follows:

$$x_{i,G}^j = x_l^j + rand().\left(x_u^j - x_l^j\right) \tag{4.10}$$

where $rand()$ symbolizes pseudo-random number between [0,1), also l and u are the lower and upper limits for each parameter.

The evolution cycle includes mutation, crossover and selection operations (Fig. 4.3). Mutation operation is run to form a donor (mutant) vector, $v_{i,G} = \left(v_{i,G}^1, v_{i,G}^2, \ldots., v_{i,G}^D\right), i = 1, 2, \ldots., Np$, for each target vector. Generally, there are five differential mutation strategies (Li and Yin 2012). Previous studies (Balkaya 2013; Ekinci 2016; Ekinci et al. 2017, 2019) are indicated that DE/best/1/bin supplies better solutions with a good estimation accuracy and less computing time for the

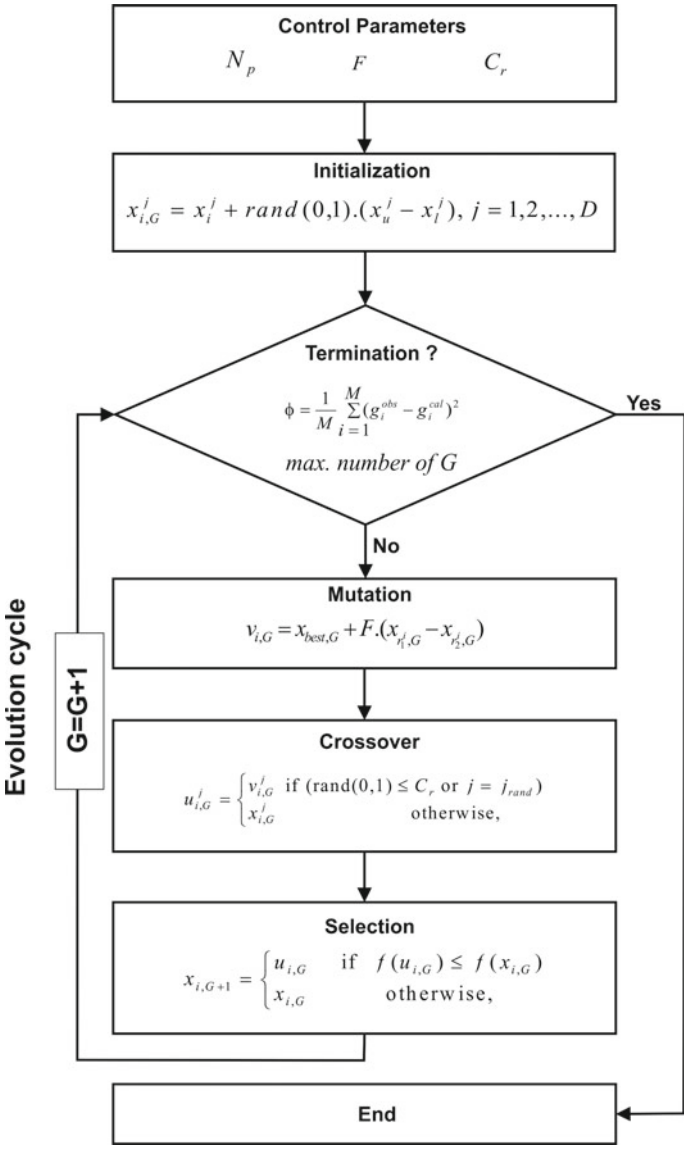

Fig. 4.3 The flow chart of the DE optimization algorithm (from Ekinci et al. 2016)

inversion of geophysical data sets. This strategy is preferred in the DE optimizations of the synthetic and field SP data in this work. Mutation operation for this strategy can be defined as below:

$$v_{i,G} = x_{best,G} + F.\left(x_{r_{1,G}^i} - x_{r_{2,G}^i}\right) \tag{4.11}$$

Here, $x_{best,G}$ is the best individual vector in the population at generation G, and (x_{r_1}, x_{r_2}) is a pair of differential vectors.

Then, the trial vector $(u_{i,G})$ is produced by a recombination of the donor vector $\left(v_{i,G}\right)$ and the target vector $(x_{i,G})$. The trail vector of the jth particle in the ith dimension at the G th iteration can be written as:

$$u_{i,G}^{j} = \begin{cases} v_{i,G}^{j} \; if \; (rand(0,1) \leq Cr \; or \; j = j_{rand}) \\ x_{i,G}^{jk} \qquad\qquad otherwise. \end{cases}, \quad j = 1, 2, \ldots, D \tag{4.12}$$

where Cr is a crossover rate in the range [0,1] and j_{rand} is a randomly chosen integer in the range [1, D].

Selection operator is employed to select the next generation between the trial and target vectors.

$$x_{i,G+1} = \begin{cases} u_{i,G} iff(u_{i,G} \leq f\left(x_{i,G}\right) \\ x_{i,G} otherwise. \end{cases} \tag{4.13}$$

If the new generated trial vector gives a better fitness value than its previous one, the target vector is updated by using Eq. 13, else it is kept in the present population. The fitness value is calculated for each particle from the objective function, and the particle with the best value is selected as the solution in the current generation.

Evolution cycle ends when a predefined termination criterion is met. This criterion can be error energy, and/or maximum number of G. So, the vector yielding the lower error energy value is chosen as an optimum solution for the optimization problem. In this study both termination criteria were used.

For the number of M data, the objective function (Relative Error) can be calculated as follows:

$$\phi = \frac{1}{M} \sum_{i=1}^{M} \left(g_i^{obs} - g_i^{cal}\right)^2 \tag{4.14}$$

where g^{obs} and g^{cal} are the observed and calculated data, respectively, and i indicates the observations. The square root of the Eq. (4.14) gives the Root Mean Square (RMS) value.

4.2.4 Parameter Estimation Studies

Synthetic noise-free and noisy (5%) infinitely long horizontal cylinder-shaped SP model anomalies are generated to test the parameter solution quality of the proposed algorithms. Then, to better analyse the pertinence of the suggested algorithms on real

data, they applied to four SP profile data, which are selected from Tamış-Çanakkale SP anomaly.

The values of the DE and PSO parameters used during the test and field studies are summarized in Table 4.1. The codes for all algorithms are written in MATLAB® (*ver.R2019a*) software with a 3.10 GHz compatible computer with 6 GB memory.

4.2.5 Synthetic Examples

First, to test the parameter solution quality of the proposed algorithms, synthetic noise-free and noisy anomalies based on an infinitely long horizontal cylinder-shaped model were generated. The parameters used for this model were selected as $K = 100\,000$ mV.m, $z_0 = 500$ m, $x_0 = 950$ m, $x_0 = 145^o$, $q = 1$, and profile length is 2000 m (assuming 50 m sampling interval) (Fig. 4.1). To calculate the noisy synthetic model, 5% Gaussian noise, were added to the synthetic data (Fig. 4.1). Thereafter the proposed algorithms have been applied for estimating the model parameters of the SP source body.

Local optimization (gradient-based) algorithms requires choose the initial parameter values close to the true solution, otherwise the algorithm may end up with a local minimum instead of a global one. To cope with this problem, a new approach to assign the initial values to the LM inversion algorithm has been introduced in this study. For this purpose, similar to the population-based metaheuristic methods, a set including 100 different models for SP have been generated randomly within certain ranges (Table 4.2), then objective function values for each model have been calculated by forward solution. Among these models the one with the lowest error energy has been taken as the initial model for LM. Finally, a LM inversion has been carried based on this initial model. Optionally this procedure may be repeated several times (Göktürkler and Balkaya 2012; Li and Yin 2012; Balkaya 2013), the one with the lowest error energy can be assigned as the solution.

Table 4.3 illustrates the initial models by the above mentioned routine for LM algorithm for noise-free and noisy SP data sets. As can be seen from the table the noisy data set produced larger RMS value as expected. The Tables 4.4 and 4.5 give the results of the parameter estimations by the LM, DE and PSO with both the noise-free

Table 4.2 Parameter ranges used to select LM algorithm initial parameters and generate the initial models by PSO and DE of noise-free and noisy synthetic SP anomalies

Parameters	True	Search Space	
		Minimum	Maximum
x_0 (m)	950	500	1000
z_0 (m)	250	100	500
θ (^{o})	145	0	180
K (mV. m$^{(2q-1)}$)	100000	10000	250000
q	1	0.5	1.5

Table 4.3 Estimated initial SP model parameters for LM algorithm by the proposed approach. This approach has been repeated 10 times, and the model having the lowest error energy has been taken as the initial model

Anomaly	RUN	Parameters					
		x_0(m)	z_0(m)	θ (°)	K (mV. m$^{(2q-1)}$)	q	RMS (mV)
Noise-free	2	904.82	465.38	142.67	167640.86	1.01	2197.28895
Noisy (5%)	2	721.55	341.32	84.28	120239.64	1.08	11271.51951

Table 4.4 The best solutions from noise-free synthetic data set by three algorithms at the end of 10 independent runs

Algorithm	RUN	Parameters					
		x_0(m)	z_0(m)	θ (°)	K (mV. m$^{(2q-1)}$)	q	RMS (mV)
DE	4	950.00	250.00	145.00	100020.65	1	0.00251022
PSO	6	949.72	248.69	144.84	95110.06	1	0.13
LM	2	950.00	250.00	144.77	100015.32	1	0.67

Table 4.5 The best solutions from noisy synthetic data set by three algorithms at the end of 10 independent runs

Algorithm	RUN	Parameters					
		x_0(m)	z_0(m)	θ (°)	K (mV. m$^{(2q-1)}$)	q	RMS (mV)
DE	7	949.34	241.83	143.51	67884.33	0.97	5.31
PSO	10	950.32	246.03	144.04	78618.48	0.98	5.32
LM	2	949.33	241.78	143.97	67762.78	0.97	5.47

and noisy SP anomalies. The comparisons of the synthetic and calculated anomalies are illustrated in Fig. 4.4. When Tables 4.4 and 4.5 are compared for noise-free data (Fig. 4.4a–c), it is observed that the algorithms generated similar results in the vicinity of true model parameters. On the other hand, the results for noisy data sets (Fig. 4.4d–f) are deviated from the true model parameters. Based on Fig. 4.4 and Tables 4.4 and 4.5, it can be said that the DE algorithm is relatively better than the others for both noise-free and noisy data sets. The behaviour of parameters and error energy variations of DE solutions are only presented in figure form (Fig. 4.5), in order to save some space in the text.

4.2.6 Field Example

Çanakkale is tectonically active region on the Alpine-Himalayan Mountain Belt that corresponds to the northward movement of the Arabian plate and located in the middle segment of the NAF zone (Altınok et al. 2012). The main fault systems of the region

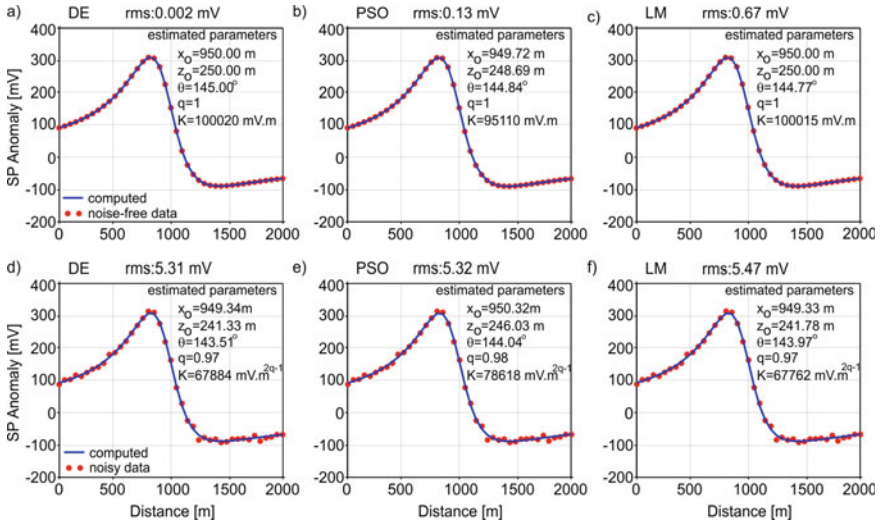

Fig. 4.4 Synthetic data: **a**–**c** Noise-free, **d**–**f** noisy data. Calculated anomalies from DE, PSO and LM algorithms (The estimated best-fitting parameters are listed on the figures)

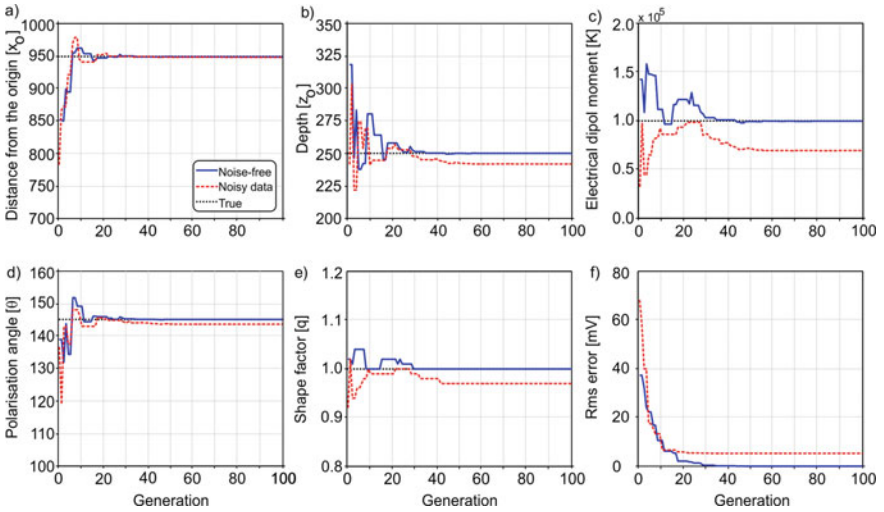

Fig. 4.5 The convergence characteristics of the DE algorithm. **a** Amplitude K, **b** the distance from the origin x_0, **c** depth z_0, **d** polarization angle θ, **e** Shape factor q

are Balabanlı, Kestanbol, Tuzla and Edremit Faults. There are a number of geothermal fields (Tuzla, Palamutova, Kestanbol, Küçükçetmi geothermal fields etc.) related with these faults in the study area. The field data sets including SP and VES in this study were collected near a segment of the Tuzla fault system. It represents the transition

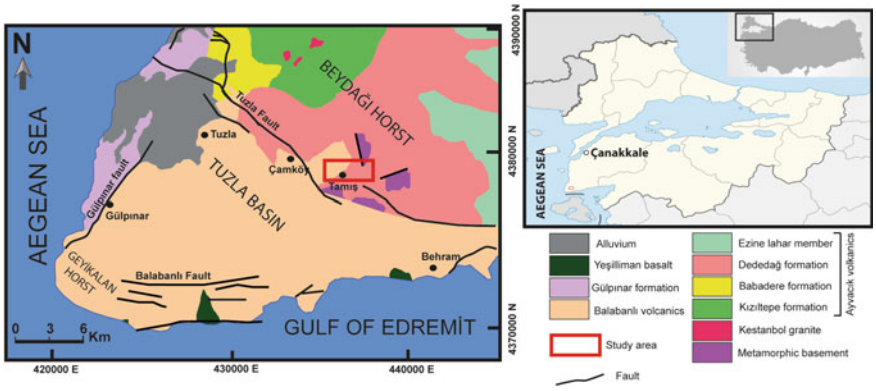

Fig. 4.6 Geological map of the study area (adapted and modified from Karacık and Yılmaz 1998; Sözbilir et al. 2018)

zone between the Beydağı Horst and Tuzla Basin. Geological units of the study area are the Balabanlı volcanics, Dededağ formations, and Karadağ metamorphics. The Balabanlı volcanics consist of pyroclastic rocks such as rhyodacitic ignimbrites and lavas. The Dededağ formation contains andesitic and trachyandesitic lavas and flow-breccias. The Balabanlı volcanics and Dededağ formation lie over the metamorphic basement (Karacık and Yılmaz 1998; Sözbilir et al. 2018) (Fig. 4.6).

The SP contour map and the superimposed locations of the VES measurements are shown in Fig. 4.7a. The VES method was carried out at five stations using the Schlumberger array. They have been inverted by a software based on a least-squares approach (IPI2WIN), and the inverted resistivity values can be seen in Fig. 4.7b. They indicate two distinct units. The first one is the surface volcanics characterized by low resistivities (10–50 Ωm), and the second one is the metamorphic units (having resistivities of 50–200 Ωm) forming the basement. It is seen that the depth to the basement ranges between approximately 350-600 m from the station VES-1 to VES-4, and the depth to the basement rock is approximately 180 m at the station VES-5. The difference between the depths may be explained as the effect of the Tuzla Fault System.

Four different profiles (P1, P2, P3, and P4) were selected for inversion (Fig. 4.7a). They have been evaluated by LM, PSO, and DE algorithms. Search spaces for these algorithms are given in Table 4.6. The procedure of assigning initial values for the LM inversion algorithm introduced in the present study (see Sect. 3.2) has also been applied to the Tamış-Çanakkale data set (Table 4.7). The same values for the algorithm-based parameters as the synthetic data evaluation were also used for the field data set. The measured and calculated data from SP profiles are given in Figs. 4.8, 4.9, 4.10 and 4.11. Tables 4.8, 4.9, 4.10 and 4.11 show the results of the model parameter estimations from the field data sets. Similar to the synthetic data, LM, PSO, and DE algorithms have been executed 10 times and the one has the minimum RMS value has been selected as the best-fitting model (Tables 4.8, 4.9, 4.10 and

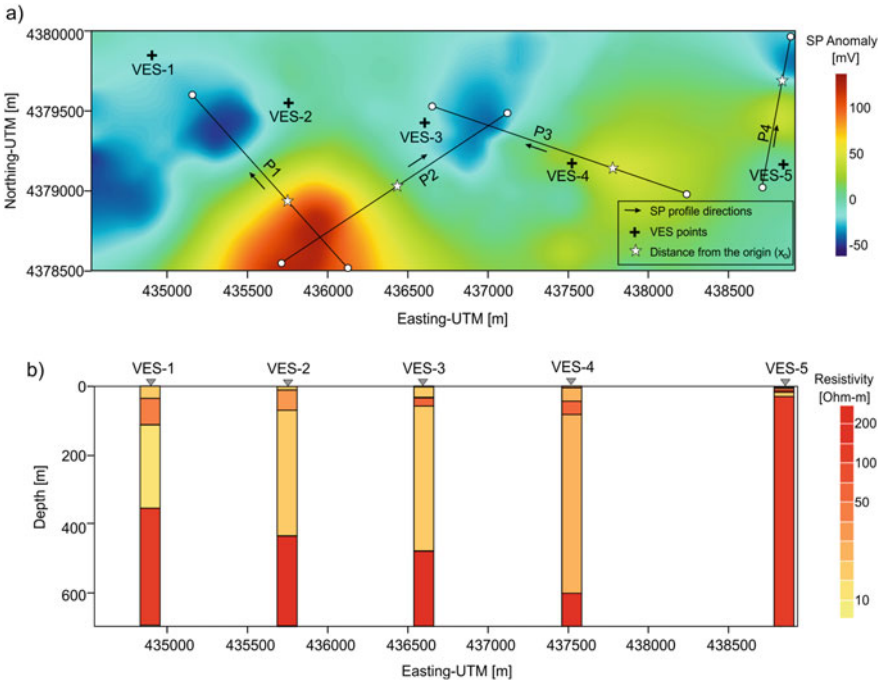

Fig. 4.7 **a** SP anomaly map, location of selected SP profiles (P1, P2, P3, and P4), VES stations (VES-1, VES-2, VES-3, VES-4, and VES-5), and estimated SP body locations (stars). **b** Layered earth models obtained from VES studies

Table 4.6 Parameter ranges used in LM, PSO and DE optimizations of the Tamış-Çanakkale anomalies

Parameters	Search Space	
	Minimum	Maximum
x_0 (m)	100	1500
z_0 (m)	100	1000
θ (°)	0	180
K (mV.m$^{(2q-1)}$)	10000	750000
Q	0.5	1.5

4.11). Although DE and PSO algorithms have smaller RMS errors than does LM with the help of the initial model determination procedure developed for the LM algorithm in this study, it is seen that the parameters are also successfully predicted with LM. When the tables are examined, it can be seen that all algorithms provided similar z_0 values (~500–700 m) for the SP profiles, except profile P4. On the other hand, the algorithms have determined a smaller z_0 values (~185 m) for P4. The calculated average depths (z_0) and origin to distances (x_0^{P1}, x_0^{P2}, x_0^{P3} and x_0^{P4}) of the SP body using by the algorithms are shown in Fig. 4.12. It is seen that there is a

Table 4.7 The initial SP parameters by the proposed approach in the present study for LM inversion of the Tamış-Çanakkale data set. This approach has been repeated 10 times, and the model having the lowest error energy has been taken as the initial model

Profile	RUN	Parameters					
		x_0(m)	z_0(m)	θ (°)	K (mV. m$^{(2q-1)}$)	q	RMS (mV)
P1	10	445.77	820.21	147.64	635087.96	1.12	272.87181
P2	9	1038.32	323.03	156.4	390919.62	1.32	551.5644
P3	4	665.56	261.31	174.41	311517.25	1.34	294.73764
P4	10	629.73	783.03	144.68	605134.85	1.1	1344.37074
Algorithm	RUN	Parameters					
		x_0(m)	z_0(m)	θ (°)	K (mV. m$^{(2q-1)}$)	q	RMS (mV)
DE	4	557.3	504.52	145.81	750000	1.18	3.22
PSO	4	556.71	500.43	145.55	634540.45	1.16	3.23
LM	10	557.43	505.62	146.37	786066.39	1.18	3.32

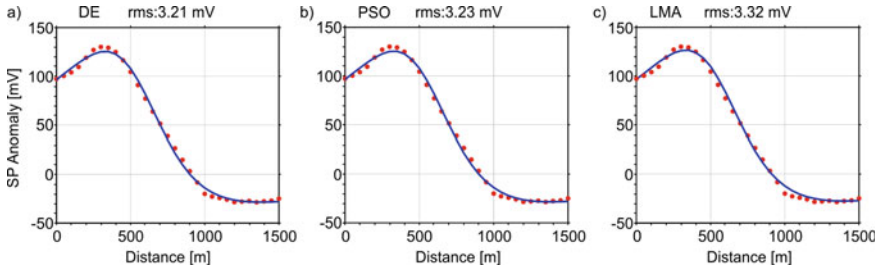

Fig. 4.8 **a** DE, **b** PSO and, **c** LM inversions of P1-profile

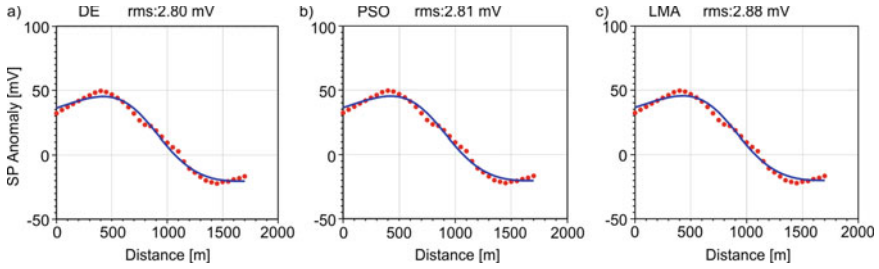

Fig. 4.9 **a** DE, **b** PSO and, **c** LM inversions of P2-profile

depth difference between the points x_0^{P3} and x_0^{P4}. Considering that the study area is in a horst-graben transition boundary, this difference may be related with the Tuzla Fault System. These findings are accordance with those of VES studies.

When we combine the geological units of the study area (Fig. 4.6) with the SP and VES findings, we can say that the surface volcanics become thinner and the

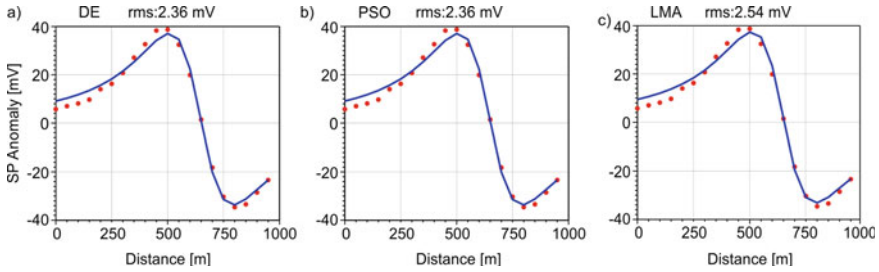

Fig. 4.10 **a** DE, **b** PSO and, **c** LM inversions of P3-profile

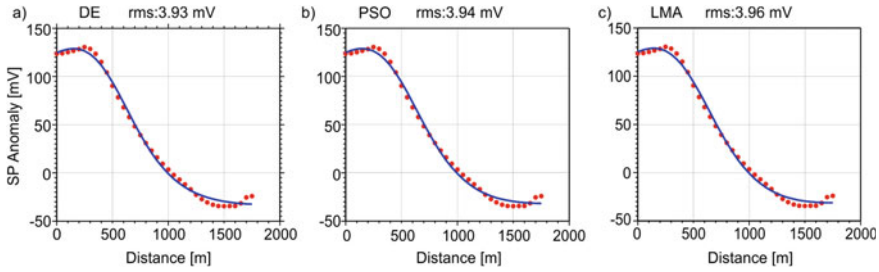

Fig. 4.11 **a** DE, **b** PSO and, **c** LM inversions of P4-profile

Table 4.8 The best solutions from Tamış-Çanakkale P1 data set by three algorithms at the end of 10 independent runs

Algorithm	RUN	Parameters					
		x_0(m)	z_0(m)	θ (°)	K (mV. m$^{(2q-1)}$)	q	RMS (mV)
DE	4	557.3	504.52	145.81	750000	1.18	3.22
PSO	4	556.71	500.43	145.55	634540.45	1.16	3.23
LM	10	557.43	505.62	146.37	786066.39	1.18	3.32

Table 4.9 The best solutions from Tamış-Çanakkale P2 data set by three algorithms at the end of 10 independent runs

Algorithm	RUN	Parameters					
		x_0(m)	z_0(m)	θ (°)	K (mV. m$^{(2q-1)}$)	q	RMS (mV)
DE	1	836.57	686.04	161.14	749999.99	1.21	2.8
PSO	5	836.51	685.93	161.14	750000	1.21	2.8
LM	9	834.49	650.39	159.91	243277.16	1.13	2.88

metamorphic basement units reach the shallower depths in the east and northeast of the study area. In the light of comparison of two geophysical methods we can said

Table 4.10 The best solutions from Tamış-Çanakkale P3 data set by three algorithms at the end of 10 independent runs

Algorithm	RUN	Parameters					
		x_0(m)	z_0(m)	θ (°)	K (mV. m$^{(2q-1)}$)	q	RMS (mV)
DE	4	480.21	633.49	140.98	37624.04	0.93	3.93
PSO	1	488.31	695.96	144.07	199675.88	1.04	3.94
LM	6	489.89	709.06	144.85	281692.89	1.07	3.96

Table 4.11 The best solutions from Tamış-Çanakkale P4 data set by three algorithms at the end of 10 independent runs

Algorithm	RUN	Parameters					
		x_0(m)	z_0(m)	θ (°)	K (mV. m$^{(2q-1)}$)	q	RMS (mV)
DE	1	644.98	185.99	177.91	750000	1.37	2.36
PSO	1	644.96	185.99	177.9	750000	1.37	2.36
LM	4	645.15	180.37	177.34	476253.67	1.33	2.54

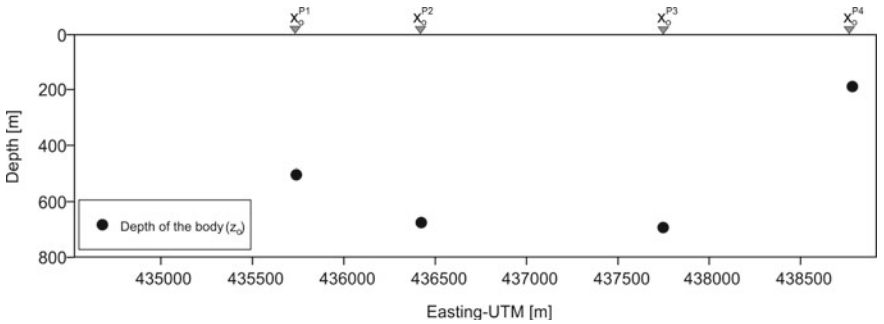

Fig. 4.12 Estimated source depths (dots) from the inversion of the SP profile data

that the depth values estimated from SP and VES methods are in good agreements with each other.

4.3 Conclusions

In this study, the model parameters of a polarized body have been determined by a derivative-based (LM), and two population-based optimization algorithms (DE and PSO), and the results are compared. Even though it is not preferred to compare derivative-based algorithms with metaheuristics, a comparison could be realized by a LM-based limitation procedure introduced in this study. By this limitation procedure,

the misfit values from the LM algorithm have been observed as being close to those from DE and PSO for both synthetic and field data sets.

In this study, Tamış-Çanakkale SP anomaly from Turkey was also evaluated with the mentioned algorithms and the solutions of them compared to each other. RMS value of the LM solution is relatively higher than the others. Comparison of the estimated SP model parameters to the VES sections has indicated that the surface volcanics become thinner and the metamorphic basement units reach the shallower depths in the east and northeast of the study area.

As a result, the solutions by DE, PSO, and LM (with limitation procedure introduced by the present study) are represented by being in good agreement with each other and they have the ability to converge from local best to the general best, can be successfully applied in determining SP model parameters. The LM algorithm, after the process introduced by the present study, has yielded results comparable with the other algorithms PSO and DE. It also displayed better convergence characteristics after the proposed process.

References

Abdelazeem M, Gobashy M (2006) Self-potential inversion using genetic algorithm. J King Abdulaziz University Earth Sci 17:83–101

Abdelrahman EM, Ammar AA, Sharafeldin SM, Hassanein HI (1997) Shape and depth solutions from numerical horizontal self-potential gradients. Appl Geophys 36:31–43

Abdelrahman EM, Ammar AA, Hassanein HI, Hafez MA (1998) Derivative analysis of SP anomalies. Geophysics 63:890–897

Abdelrahman EM, Essa KS, Abo-Ezz ER, Soliman KS, El-Araby TM (2006) A least-squares depth–horizontal position curves method to interpret residual SP anomaly profiles. J Geophys Eng 3:252–259

Abedi M, Hafizi MK, Norouzi GH (2012) 2D interpretation of self-potential data using Normalized Full Gradient, a case study: galena deposit. Bollettino di Geofisica Teorica ed Applicata 53:213–230

Agarwal BNP, Srivastava S (2009) Analyses of self-potential anomalies by conventional and extended Euler deconvolution techniques. Comput Geosci 35:2231–2238

Al-Garni M, Sundararajan, N (2011). Hartley spectral analysis of self-potential anomalies caused by a 2-D horizontal circular cylinder. Arabian J Geosci 5(6). https://doi.org/10.1007/s12517-011-0285-8

Altınok Y, Alpar B, Yaltırak C, Pınar A, Özer N (2012) The earthquakes and related tsunamis of October 6, 1944 and March 7, 1867. NE Aegean Sea Nat Hazards 60(1):3–25

Asfahani J, Tlas M, Hammadi M (2001) Fourier analysis for quantitative interpretation of self-potential anomalies caused by horizontal cylinder and sphere. J King Abdulaziz University-Earth Sci 13:41–53

Balkaya Ç (2013) An implementation of differential evolution algorithm for inversion of geoelectrical data. J Appl Geophys 98:160–175

Barnston AG (1992) Correspondence among the correlation, RMSE, and Heidke forecast verification measures; refinement of the Heidke score. Wea Forecasting 7(4):699–709

Biswas A, Sharma SP (2014) Optimization of Self-Potential interpretation of 2-D inclined sheet-type structures based on Very Fast Simulated Annealing and analysis of ambiguity. J Appl Geophys 105:235–247

Biswas A, Sharma SP (2015) Interpretation of self-potential anomaly over idealized body and analysis of ambiguity using very fast simulated annealing global optimization. Near Surface Geophysics 13:179–195

Corwin RF (1990) The self-potential method for environmental and engineering applications. In: Ward SW (ed) Geotechnical and environmental geophysics I: 127–145

Corwin RF, Hoover DB (1979) The self-potential method in geothermal exploration. Geophysics 44(2):226–245

Di Maio R, Patella D (1994) Self-potential anomaly generation in volcanic areas. Acta Vulcanol 4:119–124

Di Maio R, Piegari E, Rani P, Avella A (2016) Self-potential data inversion through the integration of spectral analysis and tomographic approaches. Geophys J Int 206:1204–1220

Di Maio R, Rani P, Piegari E, Milano L (2017) Self-potential data inversion through a Genetic-Price Algorithm. Comput Geosci 94:86–95

El-Kaliouby HM, Al-Garni MA (2009) Inversion of self-potential anomalies caused by 2D inclined sheets using neural networks. J Geophys Eng 6:29–34

Ekinci YL, Balkaya Ç, Göktürkler G, Turan S (2016) Model parameter estimations from residual gravity anomalies due to simple-shaped sources using differential evolution algorithm. J Appl Geophys 129:133–147

Ekinci YL, Özyalın Ş, Sındırgı P, Balkaya Ç, Göktürkler G (2017) Amplitude inversion of the 2D analytic signal of magnetic anomalies through the differential evolution algorithm. J Geophys Eng 14:1492–1508

Ekinci YL, Balkaya Ç, Göktürkler G (2019) Parameter estimations from gravity and magnetic anomalies due to deep-seated faults: differential evolution versus particle swarm optimization. Turk J Earth Sci 28:860–881

Essa K, Mehanee S, Smith PD (2008) A new inversion algorithm for estimating the best fitting parameters of some geometrically simple body to measured self-potential anomalies. Explor Geophys 39:155–163

Fernández-Martínez JL, García-Gonzalo E, Naudet V (2010). Particle swarm optimization applied to solving and appraising the streaming-potential inverse problem. Geophysics, 75:WA3–WA15

Fitterman DV, Corwin RF (1982) Inversion of self-potential data from the Cerro-Prieto geothermal field Mexico. Geophysics 47:938–945

Gilbert D, Pessel M (2001) Identification of sources of potential fields with the continuous wavelet transform: application to self-potential profiles. Geophys Res Lett 28:1863–1866

Göktürkler G, Balkaya Ç (2012) Inversion of self-potential anomalies caused by simple-geometry bodies using global optimization algorithms. J Geophys Eng 9(5):498–507

Göktürkler G, Balkaya Ç, Ekinci, YL Turan S (2016) Metaheuristics in applied geophysics (in Turkish). Pamukkale Univ Muh Bilim Derg., 22(6):563–580. https://doi.org/10.5505/pajes.2015.81904

Hamzah U, Samsudin AR, Malim AP (2007) Groundwater investigation in Kuala Selangor using vertical electrical sounding (VES) surveys. Environ Geol 51(8):1349–1359

IPI2 WIN Free Version 3.0.1 (2000). Program for vertical electrical sounding curves 1-D interpreting along a simple profile. Department of Geophysics, Geological Faculty, Moscow State University, Russia. http://geophys.geol.msu.ru/ipi2win.htm Accessed 16 August 2020

Juan LFM, Esperanza GG, José PFÁ, Heidi AK, César OMP (2010) PSO, a powerful algorithm to solve geophysical inverse problems, application to a 1D-DC resistivity case. J Appl Geophys 71:13–25

Juliano T, Mauriello P, Patella D (2002) Looking inside Mount Vesuvius by potential fields integrated probability tomographies. J Volcanol Geotherm Res 113:363–378

Jupp DLB, Vozoff K (1975) Stable iterative methods for the inversion of geophysical data. Geophys J Roy Astron Soc 42(3):957–976. https://doi.org/10.1111/j.1365-246x.1975.tb06461.x

Kaftan I, Sındırgı P, Akdemir Ö (2014) Inversion of self potential anomalies with multilayer perceptron neural networks. Pure appl Geophys 171:1939–1949

Karacık Z, Yılmaz Y (1998) Geology of the Ignimbrites and and the associated volcano–plutonic complex of the Ezine area, northwestern Anatolia. J Volcanol Geoth Res 85:251–264
Karlık G, Kaya MA (2001) Investigation of groundwater contamination using electric and electromagnetic methods at an open waste-disposal site: a case study from Isparta Turkey. Environ Geol 40(6):725–731
Kaya MA, Özürlan G, Balkaya Ç (2015) Geoelectrical investigation of seawater intrusion in the coastal urban area of Çanakkale. NW Turkey. Environmental Earth Sciences 73(3):1151–1160
Kennedy J, d Eberhart R (1995). Particle swarm optimisation Proceedings IEEE international conference on neural networks (Piscataway, NJ), p 1942
Levenberg K (1944) A method for the solution of certain non-linear problems in least squares. Q Appl Math 2(2):164–168. https://doi.org/10.1090/qam/10666
Li X, Yin M (2012) Application of differential evolution algorithm on self-potential data. PLoS ONE 7(12): https://doi.org/10.1371/journal.pone.0051199
Luke S (2009) Essentials of Metaheuristics (Lulu) p 233 Available free at http://cs.gmu.edu/~sean/book/metaheuristics/
Mehanee SA (2015) Tracing of paleo-shear zones by self-potential data inversion: case studies from the KTB, Rittsteig, and Grossensees graphite-bearing fault planes. Earth Planets Space 67:14. https://doi.org/10.1186/s40623-014-0174-y
Marquardt D (1963) An algorithm for least-squares estimation of nonlinear parameters. SIAM J Appl Math 11(2):431–441
Monteiro Santos FA (2010) Inversion of self-potential of Idealized bodies' anomalies using particle swarm optimization. Comput Geosci 36:1185–1190
Monteiro Santos FA, Almeida EP, Castro R, Nolasco R, Victor LM (2002) A hydrogeological investigation using EM34 and SP surveys. Earth Planets Space 54:655–662
Ogilvy AA, Ayed MA, Bogoslovsky VA (1969) Geophysical studies of water leakage from reservoirs. Geophys Prospect 17(1):36–62
Particle Swarm optimization. Introduction to Particle Swarm Optimization. http://mnemstudio.org/particle-swarm-introduction.htm. Accessed 10 Sep 2020
Patella D (1997) Introduction to ground surface self-potential tomography. Geophys Prospect 45:653–681
Paul MK (1965) Direct interpretation of self-potential anomalies caused by inclined sheets of infinite extensions. Geophysics 30:418–423
Pekşen E, Yas T, Kayman AY, Özkan C (2011) Application of particle swarm optimization on self-potential data. J Appl Geophys 75(2):305–318
Poli R, Kennedy J, Blackwell T (2007) Particle swarm optimization: an overview Swarm Intell, 1–25
Rao BSR, Murthy IVR, Reddy SJ (1970) Interpretation of self-potential anomalies of some simple geometrical bodies. Pure appl Geophys 78:60–77
Revil A, Ehouarne L, Thyreault E (2001) Tomography of self-potential anomalies of electrochemical nature. Geophys Res Lett 28(23):4363–4366
Revil A, Naudet V, Nouzaret J, Pessel M (2003) Principles of electrography applied to self-potential sources and hydrogeological applications. Water Resources Res. 39:1114. https://doi.org/10.1029/2001WR000916
Salmon S (2011). Particle Swarm Optimization in Scilab Available at http://forge.scilab.org/index.php/p/pso-toolbox/downloads/
Satyanarayana Murty BV, Haricharan P (1985) Nomogram for the complete interpretation of spontaneous potential profiles over sheet-like and cylindrical two-dimensional sources. Geophysics 50:1127–1135
Schiavone D, Quarto R (1984) Self-potential prospecting in the study of water movement. Geoexploration 22:47–58
Sharma SP (2012) VFSARES- a very fast simulated annealing FORTRAN program for interpretation of 1-D DC resistivity sounding data from various electrode array. Comput Geosci 42:177–188

Shi Y and Eberhart RC (1998). Parameter selection in particle swarm optimization Proc. 7th international conference on evolutionary programming VII (New York) pp 591–600

Sındırgı, P Özyalın Ş (2019) Estimating the location of a causative body from a self-potential anomaly using 2D and 3D normalized full gradient and Euler deconvolution. Turkish J Earth Sci 28:640–659. https://doi.org/10.3906/yer-1811-14

Sındırgı P, Pamukçu O, Özyalın Ş (2008) Application of normalized full gradient method to self potential (SP) data. Pure appl Geophys 165:409–427

Sözbilir H, Uzel B, Sümer Ö, Eski S, Softa M, Tepe Ç, Özkaymak Ç, Baba A (2018). Seismic Sources Of (14th January-20th March 2017) Çanakkale-Ayvacık Earthquake Swarm. Eskişehir Technical University Journal of Science and Technology B- Theoritical Sciences, Special Issue of 4th international earthquake engineering and seismology conference, vol 6, 1–17. https://doi.org/10.20290/aubtdb.498805

Storn R, Price KV (1995) Differential evolution-A simple and efficient adaptive scheme for global optimization over continuous spaces. Technical Report TR-95-012. International Computer Science Institute, Berkeley, CA

Storn R and Price K (1997). Differential evolution-a simple and efficient heuristic for global optimization over continuous spaces. J Glob Optim 11:341–359

Sundararajan N, Arun Kumar I, Mohan NL, Seshagiri Rao SV (1990) Use of the Hilbert transform to interpret self-potential anomalies due to two-dimensional inclined sheets. Pure appl Geophys 133:117–126

Yüngül S (1950) Interpretation of spontaneous-polarization anomalies caused by spherical ore bodies. Geophysics 15:237–246